Decoupling Analysis of Urban Growth and Carbon Emissions in Wuhan, 2000-2020

Yulian Liu[1,2], Jingwen Zhong[1,2], Zhongwei Liu[1], Youjia Liang[1,*]

[1]School of Resources and Environmental Engineering, Wuhan University of Technology, Wuhan 430070, China
[2]These authors contributed to the work equally and should be regarded as co-first authors.

Abstract. The analysis of the coupling relationship between urban growth and carbon emissions and its synergistic change rule is of great significance to the sustainable development of cities. The BCI index method is used to extract the scope of built-up areas of Wuhan from 2000 to 2020, and the relationship between urban growth and carbon emissions is analyzed based on the Tapio decoupling model. The results show that: (i) The built-up areas of Wuhan City expanded from 2000 to 2020 in all directions with Wuchang, Hankou, and Hanyang as the center, forming a stable monocentric urban spatial structure. The growth of the built-up areas exhibited stage characteristics, including a clear start, acceleration, high-speed growth, and deceleration. (ii) The carbon emissions of Wuhan City from 2000 to 2020 showed an overall growth trend. Three districts, Jiangxia, Huangpi and Hongshan, become high-emission districts, three districts, Caidian, Dongxihu and Xinzhou, become higher-emission districts, and the other seven districts maintain a lower level of carbon emissions; (iii) The carbon emissions and expansion of built-up areas in Wuhan city districts from 2000 to 2020 show obvious spatial and temporal heterogeneity. They present a decoupling of aggregation in the central area and some regression in the periphery, but the overall trend is favorable. The study provides useful references for urban planning and policy making.

1 Introduction

Urbanization refers to the process in which human life and productivity activities gradually shift from rural to urban areas as social productivity continuously develops, leading to the continuous expansion of urban space [1]. In recent years, the process of urbanization has accelerated around the world, resulting in more land being converted to construction land, and problems such as air pollution have become more prominent. Studies have shown that carbon emissions from land use changes are the second largest source of carbon globally, and the expansion of construction land is one of the important factors affecting urban carbon emissions [2].

Impervious surfaces refer to the built-up areas with a small infiltration rate in the city. During urbanization, natural landscapes are often replaced by impervious surfaces, which can indirectly reflect the degree of urban construction land expansion [3]. At present, the commonly used methods for impervious surfaces extraction mainly include spectral mixture analysis, regression modelling and spectral index-based methods [4-6]. Among them, the spectral index-based method has the advantages of automatic, fast, no parameter setting and simple calculation, and the main indices include Impervious Surface Area (ISA), Normalized Difference Impervious Surface Index (NDISI), Biological Difference Index (BDI), Biophysical Composition Index (BCI), and so on.

The Organization for Economic Cooperation and Development (OECD) introduced the concept of decoupling from the field of physics to the realm of resources and the environment in 2002. This concept is employed to gauge the extent of asynchronous change between economic development and resource consumption or environmental pressure [7]. For instance, Liu et al. applied the Tapio decoupling model to assess the decoupling index of urbanization and its impact on the ecological environment. They also analysed the reasons for decoupling differences among towns and cities concerning their ecological environments, based on various economic activities [8]. Wang et al. employed the Tapio decoupling model to deconstruct the contributions of individual industrial sectors and economic activities to the decoupling process. This was done within the context of China's economic dependence on carbon dioxide emissions [9]. Peng et al. conducted an evaluation and study of various theories, including the environmental Kuznets curve and decoupling analysis. They compared these theories in terms of their theoretical underpinnings, modeling methods, and more, demonstrating the applicability of decoupling analysis in elucidating the interaction and coupling relationship between economic growth and environmental pressure [10].

Numerous scholars have conducted extensive research on the relationship between urban growth and its impact on carbon emissions, exploring this dynamic from various perspectives. For example, Li et al. introduced the Thünen

*Corresponding author's eamil: yjliang@whut.edu.cn

© The Authors, published by EDP Sciences. This is an open access article distributed under the terms of the Creative Commons Attribution License 4.0 (https://creativecommons.org/licenses/by/4.0/).

circle theory, a valuable concept for identifying the three-tier concentric circle structure encompassing carbon emissions, sinks, and pools in a monocentric city. Their research delved into the impact of urban growth on the spatial distribution and carbon density of carbon sinks [11]. Carpio et al. conducted carbon emission accounting specific to urban expansion. They based their study on socio-economic statistics, such as neighborhood-level GDP, energy consumption, and motor vehicle ownership, to comprehensively understand the carbon emissions resulting from urban development [12]. Zheng et al. developed an index system for evaluating urban form, relying on landscape pattern indices. They combined these with a spatial error model to effectively characterize the impact of urban form on carbon emissions [13]. However, it is worth noting that most of these existing studies have predominantly focused on the overall city-level analysis. They have provided valuable insights into the broader trends. Yet, they have not delved deeply into exploring the coupling relationship between urban growth and carbon emissions, especially considering their synergistic changes over time and across different spatial dimensions.

Hence, it holds paramount importance to delve deeper into the relationship between the expansion of urban built-up areas and carbon emissions. This exploration is crucial for advancing sustainable development practices and guiding the establishment of low-carbon cities. In this study, we conducted an analysis of the spatial and temporal characteristics of urban expansion in Wuhan. This analysis was based on remote sensing images of Wuhan, spanning five-year intervals from 2000 to 2020. We employed the BCI index to extract the extent of built-up areas, and the Tapio decoupling model to assess the decoupling state between urban expansion and carbon emissions. Our goal is to provide valuable insights that can inform and guide the pursuit of low-carbon economic growth and the sustainable development of Wuhan.

2 Study area and data sources

Wuhan is located in Hubei Province, in the eastern part of the Jianghan Plain, with 13 districts under the municipal jurisdiction of Jiang'an, Jianghan, Qiaokou, Hanyang, Wuchang, Qingshan, Hongshan, Dongxihu, Hannan, Caidian, Jiangxia, Huangpi, and Xinzhou (Fig. 1). The city covers a total area of 8,569.15 km^2 and serves as the central hub of China, playing a pivotal role in the nation's transportation network. In recent years, Wuhan has witnessed a surge in urban expansion, marked by a notable incongruity between the scale of urban land use, population growth, and economic development. This incongruity has grown increasingly prominent. As a result, the analysis of urban expansion and its impact on carbon emissions in Wuhan assumes particular significance.

For this study, we utilized remote sensing image data for each five-year interval between 2000 and 2020. These images were sourced from the Geospatial Data Cloud of the Chinese Academy of Sciences (https://www.gscloud.cn/search), and additional details can be found in Table 1. Wuhan's carbon emission statistics for previous years were acquired from the China Emission Accounts and Datasets (https://www.ceads.net.cn). The statistical data on Wuhan's built-up areas were referenced from the China City Statistical Yearbook and the Wuhan Statistical Yearbook.

Table 1. Image data information

Year	Image source	Image track number	Coordinate system	Resolu tion
2000	Landsat7 ETM+	122/039 123/038 123/039	WGS84	30m
2005				
2010				
2015	Landsat8 OLI			
2020				

3 Research methods

3.1 Index extraction for built-up areas boundaries

The BCI index was proposed in 2012 [14], which follows the mechanism of the V-I-S (Vegetation-Impervious-Soil) model, i.e., it is simplified into three basic types of vegetation, impervious surfaces, and soils taking into account the strong heterogeneity of urban land cover. Compared to other indices, the BCI index has unique advantages in its use in urban areas. It is able to better differentiate between soils and high albedo built-up areas and does not rely on thermal infrared bands. The BCI index has a stronger correlation with built-up areas and is more accurate in distinguishing between soil and high albedo built-up areas than indices such as ISA [15]. In the BCI index, impervious surfaces are represented by higher positive values, vegetation is denoted by lower negative values, and soil is characterized by values close to zero. These distinct values enable the differentiation of these three types of features. Calculating the BCI index involves three key steps: image preprocessing, water body masking, tasseled cap transformation, and subsequent normalization. The BCI index is determined using the following formula:

$$H = \frac{TC1 - TC1_{min}}{TC1_{max} - TC1_{min}} \tag{1}$$

$$V = \frac{TC2 - TC2_{min}}{TC2_{max} - TC2_{min}} \tag{2}$$

$$L = \frac{TC3 - TC3_{min}}{TC3_{max} - TC3_{min}} \tag{3}$$

$$BCI = \frac{\frac{H + L}{2} - V}{\frac{H + L}{2} + V} \tag{4}$$

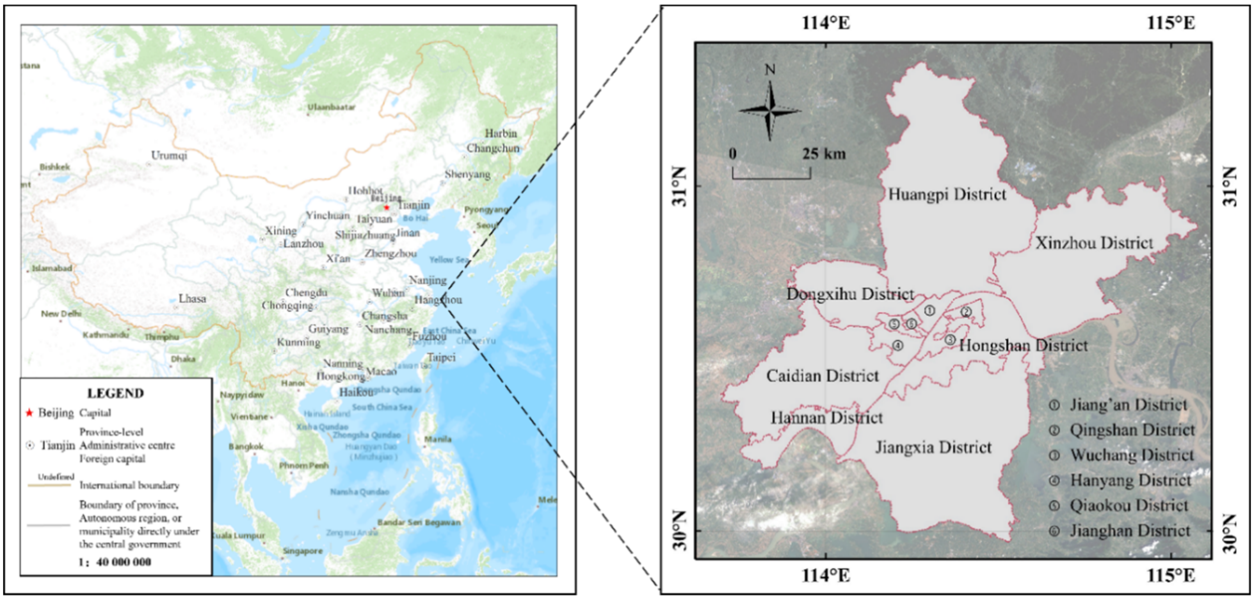

Fig. 1. Location map of Wuhan

Where H is the high albedo component, V is the vegetation component, L is the low albedo component, TCi $(i = 1,2,3)$is the luminance, greenness and humidity component of the remote sensing image after tasseled cap transformation, and TCi_{min} and TCi_{max} are the minimum and maximum values of the ith TC component, respectively.

To extract impervious surfaces using the BCI index, it is necessary to exclude water bodies. In this study, we employed the Modified Normalized Difference Waterbody Index (MNDWI) for water body masking. MNDWI is a widely adopted method that substitutes the mid-infrared band for the near-infrared band, making the differentiation between building indices and water body indices more distinct. This technique has found application in various studies, including global water body extraction [16]. The calculation of MNDWI is as follows:

$$MNDWI = \frac{Green - MWIR}{Green + MWIR} \tag{5}$$

Where $Green$ denotes the reflectance of the green light band of the image; $MWIR$ denotes the reflectance of the mid-infrared band of the image.

3.2 Tapio decoupling analysis

Two commonly used decoupling models are the OECD decoupling index model and the Tapio decoupling state analysis model [17]. The Tapio decoupling model represents an enhancement of the OECD decoupling model. It offers advantages, such as mitigating the sensitivity of the OECD model to base period selection and reducing the volatility of calculation results. As a result, it has gained widespread adoption. For example, Li et al. analysed the relationship between carbon emissions and urban land growth based on the Tapio decoupling model using the Yangtze River Delta urban agglomeration as examples [18]. In this study, we have opted to utilize the Tapio decoupling index method for analysis, employing the following calculation formula:

$$TD = \frac{\frac{\Delta C}{C_{t-n}}}{\frac{\Delta L}{L_{t-n}}} = \frac{\frac{(C_t - C_{t-n})}{C_{t-n}}}{\frac{(L_t - L_{t-n})}{L_{t-n}}} = \frac{\%\Delta C}{\%\Delta L} \tag{6}$$

Where TD denotes the Tapio decoupling index of built-up areas expansion and carbon emissions; C_t and C_{t-n} denote the total carbon emissions in the calculation period and the previous period, respectively, and $\%\Delta C$ denotes the growth rate of environmental pressure; L_t and L_{t-n} denote the total built-up areas in the calculation period and the previous period, respectively, and $\%\Delta L$ denotes the growth rate of the economic driving force. Based on the positivity and negativity of $\%\Delta C$ and $\%\Delta L$ as well as the magnitude of the Tapio decoupling index, the Tapio decoupling status is categorized into eight categories, as shown in Table 2. Fig. 2 gives the distribution of %ΔC, %ΔL, TD and decoupling status quadrants.

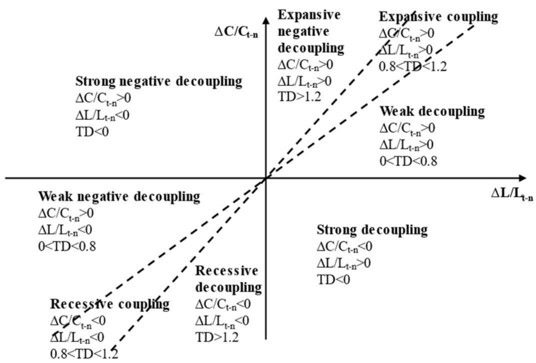

Fig. 2. Quadrant diagram of decoupled states

4 Analysis of results

The scope of built-up areas in Wuhan from 2000 to 2020 is shown in Fig. 3. Given the extensive scope of this study, assessing the accuracy of the extracted built-up area results via field measurements would be challenging. Therefore, we employed a more authoritative source, the

Table 2. Tapio decoupling index division

Decoupling state		%ΔC	%ΔL	Tapio decoupling index
Negative decoupling	Expansive negative decoupling	> 0	> 0	1.2 < TD
	Weak negative decoupling	< 0	< 0	0 ≤ TD < 0.8
	Strong negative decoupling	> 0	< 0	TD < 0
Coupling	Expansive coupling	> 0	> 0	0.8 ≤ TD < 1.2
	Recessive coupling	< 0	< 0	0.8 ≤ TD < 1.2
Decoupling	Weak decoupling	> 0	> 0	0 ≤ TD < 0.8
	Strong decoupling	< 0	> 0	TD < 0
	Recessive decoupling	< 0	< 0	1.2 < TD

Table 3. Extracted area of Wuhan built-up areas and statistical yearbook data

Year	Built-up area(km^2)			Growth rate of built-up area(%)
	Yearbook data	Extracted results	Increment	
2000	210	252.4	-	-
2005	220	336.31	83.91	33.24
2010	500	491.09	154.78	46.02
2015	755	849.36	358.27	72.95
2020	885	1017.13	167.77	19.75

statistical yearbook data, to validate the accuracy of our built-up area extraction. The results of this comparison are presented in Table 3, which demonstrates a high level of consistency between the extracted built-up areas and the yearbook data. This level of accuracy aligns with the research requirements.

4.1 Spatial and temporal characterization of Wuhan's urban growth

The standard deviation ellipse is a valuable tool for capturing the spatial characteristics of geographic elements, including central trends, dispersion, and directional patterns. Utilizing ArcGIS software, we generated corresponding standard deviation ellipses for the built-up area data from 2000 to 2020, as depicted in Fig. 3. The analysis reveals that the expansion of Wuhan City's built-up areas from 2000 to 2020 follows a dispersed pattern, with Wuchang, Hankou, and Hanyang serving as central growth points. This expansion has led to the establishment of a stable, single-centered spatial structure. The growth of built-up areas exhibited distinct stage characteristics during this period. Specifically:

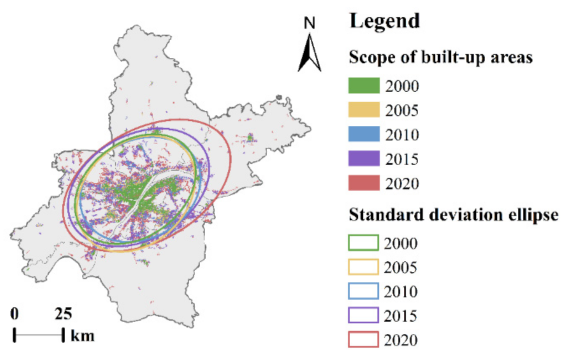

Fig. 3. Spatial Distribution and Morphology of Built-up Areas in Wuhan, 2000-2020

- From 2000 to 2005 marked the initial stage of growth, with expansion primarily towards the southwest and southeast. However, the growth rate was relatively low, with an average annual increase of only 17.25 km^2.
- The period from 2005 to 2010 saw accelerated growth, as built-up areas expanded towards the southeast and northwest, with an average annual increase of 32.68 km^2.
- Between 2010 and 2015, built-up areas expanded in all directions, with a substantial increase of 76.21 km^2 annually, representing the maximum growth rate.
- From 2015 to 2020, the expansion of built-up areas was more modest, occurring primarily in the northwestern and southwestern directions, with an average annual increase of 33.62 km^2. During this period, the growth rate decreased.

4.2 Analysis of changes in carbon emissions in Wuhan

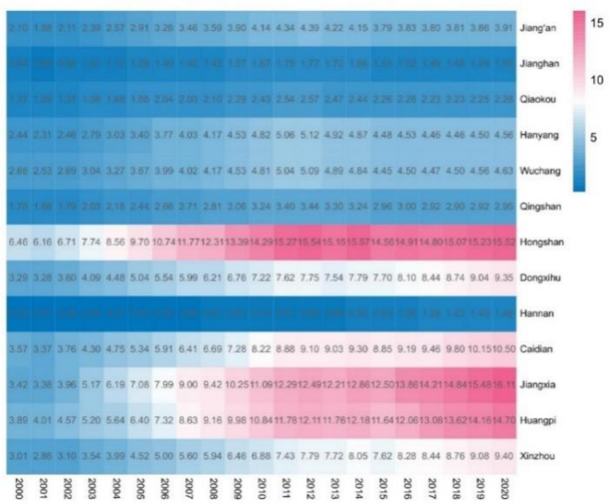

Fig. 4. Changes in carbon emissions (million tons) in Wuhan from 2000 to 2020

Carbon emissions data are non-stationary series characterized by dependence, also known as exhibiting weak smoothness. This means that the value at a future moment depends on its past information. The Autoregressive Integrated Moving Average (ARIMA) model is a time series forecasting method suitable for short-term forecasting when sufficient data samples are available [19]. Since the county-scale carbon emissions data in the China Emission Accounts and Datasets extend only up to 2017, we have employed the ARIMA model to estimate the carbon emissions data for Wuhan's administrative districts in 2020, using historical carbon emissions data from 1997 to 2017. Fig. 4 illustrates that the overall carbon emissions in Wuhan City exhibit a growth trend from 2000 to 2020. The period from 2000 to 2010 represents a growth phase. During this period, three districts—Jiangxia, Huangpi, and Hongshan—experienced the fastest growth rate in carbon emissions, classifying them as high-emission zones within Wuhan City. Concurrently, the three districts of Caidian, Dongxihu, and Xinzhou demonstrated a faster growth rate, categorizing them as higher-emission zones. The remaining seven districts maintained lower levels of carbon emissions, designating them as low-emission zones. The period from 2010 to 2020 represents a phase of fluctuating growth. During this time, carbon emissions in Hongshan and the seven low-emission districts remained stable and exhibited an overall decreasing trend. Meanwhile, the other two high-emission districts and three higher-emission districts continued to experience some growth.

4.3 Analysis of urban growth-carbon emission decoupling in Wuhan city

Wuhan's carbon emissions and built-up areas and decoupling status in each period are shown in Table 4. From 2000 to 2020, the structure of the study area as a whole changes from being dominated by expansive negative decoupling to being dominated by strong decoupling, i.e., as the built-up areas expanded, carbon emissions only rise less or even realize a decline, with an overall positive trend. Among them, five districts, namely Jiang'an, Qiaokou, Hanyang, Wuchang and Qingshan, experienced a slowdown in urban growth and a significant decline in carbon emissions, realizing a shift from expansive negative decoupling to strong decoupling; and three districts, namely Hongshan, Dongxihu and Xinzhou, experienced a significant slowdown in urban growth and the rate of growth of carbon emissions peaked in 2010, realizing a shift from expansive negative decoupling / expansive coupling to weak decoupling. While Hannan, Caidian, and Huangpi appear to oscillate between states of expansive negative decoupling, expansive coupling and weak decoupling, with Jianghan changing from a strong decoupling to a recessive decoupling in the latter two stages, Jiangxia changing from a weak decoupling to a strong negative decoupling in the latter two stages, and Hannan and Caidian both changing from a weak decoupling in the 2010-2015 period to expansive negative decoupling in the 2015-2020 period. By 2020, nine districts have already achieved decoupling between carbon emissions and built-up areas expansion, i.e., carbon emissions reductions were realized while urban construction was underway, with Jiang'an, Qiaokou, Hanyang, Wuchang and Qingshan Districts taking the lead in achieving a strong decoupling and the most desirable state of the relationship between carbon emissions and built-up areas expansion.

The spatial distribution of the decoupling status of urban growth and carbon emissions in Wuhan from 2000 to 2020 is illustrated in Fig. 5. Overall, the decoupling status of carbon emissions and built-up area expansion tended to be relatively homogeneous during 2000-2015, but this status exhibited periods of regression and improvement. It shifted from a predominantly negative decoupling status in 2005-2010 to full decoupling realization in 2010-2015. It shifted from a predominantly negative decoupling status in 2005-2010 to full decoupling realization in 2010-2015.

Specifically, from 2000 to 2005, the decoupling of carbon emissions from built-up area expansion was dominated by weak decoupling and expansive negative decoupling. During this period, there was a cluster of municipal districts exhibiting weak decoupling, an aggregation of internal municipal districts with expansive negative decoupling, and only the peripheral Hannan district was in an expansive coupling state. Between 2005 and 2010, the number of municipal districts showing expansive negative decoupling expanded, with only Dongxihu and Caidian districts in a state of expansive coupling, while the remaining municipal districts continued to experience expansive negative decoupling, resulting in an overall regression of decoupling across the region. In 2010-2015, the decoupling situation in Wuhan reached its most favorable state during the study period. This period was characterized by a majority of municipal districts showing weak decoupling on the periphery, surrounded by strong decoupling municipal districts on the inside. In particular, Jiang'an, Jianghan, Qiaokou, Hanyang, Wuchang, and Qingshan districts exhibited strong decoupling, with Jianghan District being the most highly decoupled. However, from 2015 to 2020, regional differences in decoupling status within Wuhan began to increase, with extreme states such as strong negative decoupling appearing. Except for eight districts—Jiang'an, Qiaokou, Hanyang, Wuchang, Qingshan, Hongshan, Dongxihu, and Xinzhou—maintaining good decoupling status from the previous period, the remaining five municipal districts experienced varying degrees of decoupling regression, leading to increased heterogeneity in the study area's decoupling status.

5 Discussion and conclusions

The paper used the BCI index to extract the extent of built-up areas in Wuhan from 2000 to 2020. It analyzed the coupling relationship between urban growth and carbon emissions in Wuhan, based on the Tapio decoupling model. The main conclusions are as follows: (i) Urban Expansion and Spatial Structure: The built-up areas of Wuhan expanded from 2000 to 2020, with Wuchang, Hankou, and Hanyang at its core. This expansion formed a stable single-centered urban spatial structure. The growth of built-up areas exhibited distinct stages, characterized by initial growth, acceleration, high-speed expansion, and eventual deceleration. (ii) Carbon

Table 4. Tapio decoupling index division

Districts	2000-2005				2005-2010				2010-2015				2015-2020			
	%ΔC	%ΔL	TD	State	%ΔC	%ΔL	TD	State	%ΔC	%ΔL	TD	State	%ΔC	%ΔL	TD	State
Jiang'an	0.385	0.169	2.669	END	0.424	0.193	2.199	END	-0.085	0.130	-0.651	SD	-0.030	0.106	-0.286	SD
Jianghan	0.371	0.074	5.403	END	0.294	0.038	7.799	END	-0.095	0.028	-3.427	SD	-0.083	-0.008	9.779	RD
Qiaokou	0.371	0.098	4.136	END	0.294	0.122	2.413	END	-0.071	0.103	-0.694	SD	-0.066	0.049	-1.343	SD
Hanyang	0.396	0.188	2.499	END	0.417	0.296	1.409	END	-0.072	0.465	-0.155	SD	-0.046	0.204	-0.227	SD
Wuchang	0.379	0.106	3.956	END	0.310	0.058	5.391	END	-0.076	0.045	-1.674	SD	-0.022	0.009	-2.312	SD
Qingshan	0.374	0.126	3.347	END	0.327	0.139	2.362	END	-0.088	0.130	-0.680	SD	-0.075	0.119	-0.631	SD
Hongshan	0.502	0.660	1.261	END	0.473	0.711	0.665	WD	0.019	0.912	0.021	WD	0.003	0.309	0.009	WD
Dongxihu	0.528	0.857	1.144	EC	0.435	0.755	0.576	WD	0.066	0.943	0.070	WD	0.219	0.694	0.315	WD
Hannan	0.438	0.143	3.492	END	0.789	0.844	0.934	EC	0.250	1.328	0.188	WD	1.054	0.645	1.634	END
Caidian	0.497	1.468	0.836	EC	0.539	0.727	0.742	WD	0.076	1.264	0.060	WD	0.146	0.065	2.242	END
Jiangxia	1.069	1.056	2.081	END	0.566	1.680	0.337	WD	0.127	1.753	0.073	WD	0.271	-0.055	-4.966	RD
Huangpi	0.648	0.482	1.991	END	0.693	1.123	0.617	WD	0.074	1.305	0.057	WD	0.307	0.280	1.099	EC
Xinzhou	0.501	0.515	1.475	END	0.521	1.009	0.516	WD	0.109	1.189	0.091	WD	0.193	0.331	0.583	WD

Note: END=Expansive negative decoupling; EC=Expansive coupling; SD=Strong decoupling; WD=Weak decoupling; RD=Recessive decoupling.

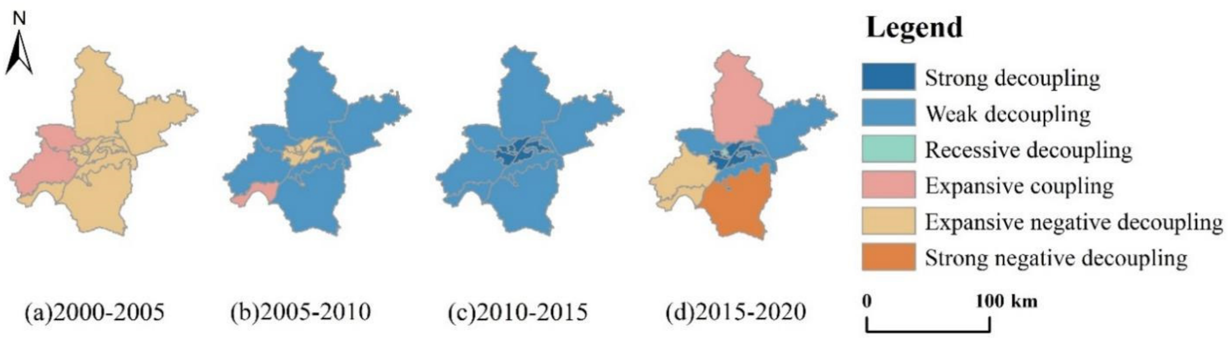

Fig. 5. Changes in carbon emissions (million tons) in Wuhan from 2000 to 2020

Emissions: Carbon emissions in Wuhan increased from 2000 to 2020. Notably, three districts—Jiangxia, Huangpi, and Hongshan—emerged as high-emission areas. (iii) Spatio-Temporal Heterogeneity: The relationship between carbon emissions and urban expansion in Wuhan's districts from 2000 to 2020 displayed clear spatio-temporal heterogeneity. Decoupling was more prominent in the central districts, while some peripheral areas experienced regression. Overall, a positive trend of decoupling was observed.

The research is of reference significance for the development strategy of low-carbon cities and urban planning. However, the study is limited to discussions within specific time periods and regions, and further in-depth research is needed on issues such as the direction of influence, elastic changes, and spatiotemporal heterogeneity. Meanwhile, the coupling of carbon emission sources with urban expansion has not beenthoroughly studied, and future studies can further explore this to provide more detailed guidance and recommendations. In addition, the conclusions of the study are related to the extraction accuracy of the built-up areas in Wuhan city, and for improved reliability, subsequent research can adopt methods with higher precision.

Acknowledgments

This paper is one of the phase results of " Carbon Emission Estimation of (2000-2060) Chinese Urban Expansion by Coupling Neural Network and Cellular Automata" (S202310497280), the National innovation and entrepreneurship training program for college students.

References

1. Liu, J., Kuang, W., Zhang, Z., et al. (2014) Spatiotemporal characteristics, patterns, and causes of land-use changes in China since the late 1980s. J. Geogr. Sci., 24: 195-210.
2. Yu, X., Chen, N., Li, M. (2020) Research on carbon emission characteristics and reduction pathways of low-carbon pilot cities in China. Chinese J. Popul. Resour. Environ., 30(07): 1-9.
3. Xu, H. (2009) Quantitative analysis on the relationship of urban impervious surface with other components of the urban ecosystem. Acta Ecol. Sin., 29(5): 2456-2462.
4. Xu, H., Wang, M. (2016) Remote sensing-based retrieval of ground impervious surfaces. J. Remote Sens., 20(5): 1270-1289.
5. Powell, R., Roberts, D., Dennison, P., et al. (2007) Sub-pixel mapping of urban land cover using multiple endmember spectral mixture analysis: Manaus, Brazil. Remote Sens. Environ., 106(2): 253-267.
6. Bauer, M., Loffelholz, B., Wilson, B. (2007) Estimating and mapping impervious surface area by regression analysis of Landsat imagery. Remote sensing of impervious surfaces, Boca Raton. pp. 31-48.
7. OECD (2002) Indicators to Measure Decoupling of Environmental Pressure from Economic Growth. OECD, Paris.
8. Liu, H., Yang, Q., Zhang, Y. (2016) Urbanization ecological environment effect in Northeast China based on decoupling analysis. Sci. Geogr. Sin., 36(12): 1860-1869.
9. Wang, Q., Zhang, R. (2019) Is China's economic growth decoupled from carbon emissions? J. Cleaner Prod., 225: 1194-1208.
10. Peng, H., Guo, L., Zhang, J., et al. (2020) Research progress and implication of the relationship between regional economic growth and resource—Environmental pressure. Resour. Sci., 42(4): 593-606.
11. Li, Z., Zhong, J., Sun, Z., et al. (2017) Spatial Pattern of Carbon Sequestration and Urban Sustainability: Analysis of Land-Use and Carbon Emission in Guang'an, China. Sustainability, 9(11): 1951.
12. Carpio A., Ponce-Lopez R, Lozano-Garcia D F. (2021) Urban form, land use, and cover change and their impact on carbon emissions in the Monterrey Metropolitan area, Mexico. Urban Clim., 39: 100947.
13. Zheng, S., Huang, Y., Sun, Y. (2022) Effects of Urban Form on Carbon Emissions in China: Implications for Low-Carbon Urban Planning. Land, 11(8): 1343.
14. Deng, C., Wu, C. (2012) BCI: A biophysical composition index for remote sensing of urban environments. Remote Sens. Environ., 127(5): 247-259.
15. Zhang, L., Weng, Q. (2016) Annual dynamics of impervious surface in the Pearl River Delta, China, from 1988 to 2013, using time series Landsat imagery. ISPRS J. Photogramm. Remote Sens., 113: 86-96.
16. Feng, M., Sexton, J O, Channan, S, et al. (2016) A global, high-resolution (30-m) inland water body dataset for 2000: First results of a topographic-spectral classification algorithm. Int. J. Digital Earth, 9(2): 113-133.
17. Tapio, P. (2005) Towards a Theory of Decoupling: Degrees of Decoupling in the EU and the Case of Road Traffic in Finland Between 1970 and 2001. J. Transp. Policy, 12: 137-151.
18. Li, Y., Gao, X., Yao, S., et al. (2022) Decoupling Relationship Between Carbon Balance Pressure and New Urbanization in the Core Area of the Yangtze River Delta Urban Agglomeration, China. Econ. Geogr., 42(12): 72-81.
19. Li, Z., Liu, S. (2019) Prediction Comparison Based on ARIMA Model, Grey Model and Regression Mode. Stat. Decis., 35(23): 38-41.